



1 **Diurnal variation in the isotope composition of plant xylem**  
2 **water biases the depth of root-water uptake estimates**

3 Hannes P.T. De Deurwaerder <sup>(1,2)\*</sup>, Marco D. Visser <sup>(2)</sup>, Matteo Detto <sup>(2)</sup>, Pascal Boeckx <sup>(3)</sup>,  
4 Félicien Meunier <sup>(1,4)</sup>, Liangju Zhao <sup>(5,6)</sup>, Lixin Wang <sup>(7)</sup>, Hans Verbeeck <sup>(1)</sup>

5 (1) CAVElab - Computational & Applied Vegetation Ecology, Faculty of Bioscience Engineering, Ghent  
6 University, Ghent, Belgium

7 (2) Department of Ecology and Evolutionary Biology, Princeton University, Princeton, NJ, USA

8 (3) ISOFYS – Isotope Bioscience Laboratory, Faculty of Bioscience Engineering, Ghent University, Ghent,  
9 Belgium

10 (4) Ecological Forecasting Lab, Department of Earth and Environment, Boston University, Boston,  
11 Massachusetts, USA

12 (5) Shaanxi Key Laboratory of Earth Surface System and Environmental Carrying Capacity, College of  
13 Urban and Environmental Sciences, Northwest University, Xi'an 710127, China

14 (6) Key Laboratory of Ecohydrology and Integrated River Basin Science, Northwest Institute of Eco-  
15 Environment and Resources, Chinese Academy of Sciences, Lanzhou 730000, China

16 (7) Department of Earth Sciences, Indiana University-Purdue University Indianapolis (IUPUI),  
17 Indianapolis, IN 46202, USA

18

19 *Correspondence to:* Hannes De Deurwaerder (Hannes\_de\_deurwaerder@hotmail.com)

20

21 **Abstract**

22 1. Stable isotopologues of water are a widely used tool to derive the depth of root water  
23 uptake (RWU) in lignified plants. Uniform isotope composition of plant xylem water  
24 (*i-H<sub>2</sub>O-xyl*) along the stem length is a central assumption, which has never been properly  
25 evaluated.



- 26 2. We studied the effects of diurnal variation in RWU, sap flux density and various other  
27 soil and plant parameters on *i-H<sub>2</sub>O-xyl* within a plant using a mechanistic plant hydraulic  
28 model and empirical field observations from French Guiana and northwestern China.
- 29 3. Our model predicts significant *i-H<sub>2</sub>O-xyl* variation arising from diurnal RWU  
30 fluctuations and vertical soil water heterogeneity. Moreover, significant differences in  
31 *i-H<sub>2</sub>O-xyl* emerge between individuals with different sap flux densities. In line with  
32 model predictions, field data show excessive *i-H<sub>2</sub>O-xyl* variation during the day or along  
33 stem length ranging up to 25.2‰ in  $\delta^2\text{H}$  and 6.8‰ in  $\delta^{18}\text{O}$ , largely exceeding the  
34 measurement error range.
- 35 4. Our work show that the fundamental assumption of uniform *i-H<sub>2</sub>O-xyl* is violated both  
36 theoretically and empirically and therefore a real danger exists of significant biases  
37 when using stable water isotopologues to assess RWU. We propose to include  
38 monitoring of sap flow and soil water potential for more robust RWU depth estimates.

39  
40 **Keywords**

41 Deuterium, Ecohydrology, Lianas, Root water uptake, Sap flow, Stable isotope composition  
42 of water, Tropical trees, Water competition

43  
44 **1. Introduction**

45 The use of stable isotope composition of water has greatly enhanced ecohydrology studies by  
46 providing insights into phenomena that are otherwise challenging to observe, such as depth of  
47 root water uptake (RWU) (Rothfuss & Javaux, 2017), below ground water competition and  
48 hydraulic lift (Hervé-Fernández *et al.*, 2016; Meunier *et al.*, 2017). Compared to root  
49 excavation, the technique is non-destructive, far less labor-intensive and informs on actual



50 RWU while excavation solely informs on root distribution and architecture. Moreover, its  
51 flexibility allows use across multiple scales both spatial (i.e. individual to ecosystem) and  
52 temporal (i.e. daily to seasonal; Dawson *et al.* 2002). The advantages and wide applicability of  
53 this method make it a popular technique that pushes the boundaries of ecohydrology (Dawson  
54 *et al.*, 2002; Yang *et al.*, 2010; Rothfuss & Javaux, 2017).

55 A variety of methods exist that infer RWU depth from the isotope composition of plant  
56 xylem water (*i-H<sub>2</sub>O-xyl*), but all rely on a direct relationship between the isotopic compositions  
57 of plant xylem water and soil water (Ehleringer & Dawson, 1992). More precisely, all have two  
58 key assumptions. The first is that the isotope composition of plant xylem water remains  
59 unchanged during transport from root uptake to evaporative sites (e.g. leaves and non-lignified  
60 green branches). Hence, isotope fractionation - processes that shift the relative abundance of  
61 the water isotopologues during root water uptake and water through non-evaporative tissues - is  
62 neglected (Wershaw *et al.*, 1966; Zimmermann *et al.*, 1967; White *et al.*, 1985; Dawson &  
63 Ehleringer, 1991; Walker & Richardson, 1991; Dawson *et al.*, 2002; Zhao *et al.*, 2016). Second,  
64 all methods assume that xylem water provides a well-mixed isotope composition of water from  
65 different soil layers: sampled xylem water instantaneously reflects the distribution and water  
66 uptake of the roots independent of sampling time or height.

67 The first assumption is relatively well supported. Fractionation at root level has not  
68 raised concerns for most RWU assessments using water isotopologues (Rothfuss & Javaux,  
69 2017), with the exception of kinetic fractionation. Kinetic fractionation is a process driven by  
70 the differences in molecule mass among the isotopologues that occurs only in extreme  
71 environments (Lin & Sternberg, 1993; Ellsworth and Williams, 2007; Zhao *et al.*, 2016).  
72 Similarly, isotopic fractionation of water within an individual plant, although possible, is not  
73 considered a serious problem (Yakir, 1992; Dawson & Ehleringer, 1993; Cernusak *et al.*, 2005;  
74 Mamonov *et al.*, 2007; Zhao *et al.*, 2016). However, the second assumption of time and space



75 invariance of the isotope composition of xylem water has, to our best knowledge, never been  
76 assessed.

77         In principle, temporal variance in  $i\text{-H}_2\text{O}\text{-xyl}$  within a plant during a day or along its height  
78 can be expected on first principles. Here we hypothesize that it is in fact likely that various plant  
79 physiological processes, ranging from very simple to more complex mechanisms could  
80 influence within plant variance in  $i\text{-H}_2\text{O}\text{-xyl}$  at short time scales. For instance, plant  
81 transpiration during the course of the day is regulated by atmospheric water demand and leaf  
82 stomata which have clear and well known diurnal patterns (Steppe & Lemeur, 2004; Epila *et*  
83 *al.*, 2017). This results in changing water potential gradients within the soil-plant-atmosphere  
84 continuum and therefore fluctuations in the depth RWU are also expected (Goldstein *et al.*,  
85 1998; Doussan *et al.*, 2006; Huang *et al.*, 2017). Hence, as we expect plants capacity to take up  
86 water at different soil layers to shift during the day, we should also expect diurnal variation in  
87 the mixture of isotope composition from water taken up from various depths. As water moves  
88 up along the xylem with velocity proportional to sap flow, different plants and species might  
89 respond differently to diurnal variation in RWU. Therefore, from very basic principles we may  
90 expect temporal variation in  $i\text{-H}_2\text{O}\text{-xy}$  to propagate to different plant heights. As sap flux density  
91 depends on plant hydraulic traits in relation to atmospheric water demand and soil moisture  
92 gradient, this mechanism could make comparison of isotopic data among individuals and  
93 species misleading.

94         In this study we provide a critical assessment of the assumption of  $i\text{-H}_2\text{O}\text{-xyl}$  invariance  
95 over time and along the length of plant stems. We test the hypothesis that major alterations in  
96 the  $i\text{-H}_2\text{O}\text{-xyl}$  along the length of lignified plants arise naturally during the day and that this  
97 variation in  $i\text{-H}_2\text{O}\text{-xyl}$  exceeds the expected measurement error. We test this hypothesis with a  
98 twofold approach. First, we build a simple mechanistic model that incorporates basic plant  
99 hydraulic realism. We use this model to specifically test that even rudimentary mechanistic



100 models of plant hydraulic functioning predict that diurnal changes in the soil-plant-atmosphere  
101 continuum result in shifting mixtures of soil water absorption differing in isotope composition.  
102 Second, we test whether the  $i\text{-H}_2\text{O}\text{-xyl}$  sampled at different plant heights or at different times  
103 of the day show large variances with field observations from i) six Neotropical canopy trees  
104 and six Neotropical canopy lianas sampled at different heights in French Guiana, and ii) high  
105 temporal resolution  $i\text{-H}_2\text{O}\text{-xyl}$  data of 6 distinct plant species from the Heihe River Basin in  
106 northwestern China (Zhao *et al.*, 2014).

107

## 108 **2. Materials and Methods**

### 109 **2.1. Part A: Modelling exploration**

#### 110 **2.1.1. Model derivation**

111 The expected  $i\text{-H}_2\text{O}\text{-xyl}$  at different stem heights within a tree during the course of the day can  
112 be derived from plant and physical properties such as root length density, total fine root surface  
113 area, water potential gradients and the isotope composition of soil water. We call this the  
114 SWIFT model (i.e. Stable Water Isotopic Fluctuation within Trees). To derive the SWIFT  
115 model, we first describe the establishment of  $i\text{-H}_2\text{O}\text{-xyl}$  entering the tree at stem base via a  
116 multi-source mixing model (Phillips & Gregg, 2003). We subsequently consider vertical water  
117 transport within the tree, which relates to the established sap flow pattern. Note that the model  
118 presented here, focusses on deuterium but can easily be used to study stable oxygen  
119 isotopologues. To ensure consistency and clarity in variable declarations we maintain the  
120 following notation in the subscripts of variables: uppercase roman to distinguish the medium  
121 through which water travels (X for xylem, R for root, S for soil) and lowercase for units of time  
122 and distance ( $h$  for stem height,  $t$  for time and  $i$  for soil layer index). A comprehensive list of



123 variables, definitions and units is given in Table 1. A schematic representation of the model is  
124 provided in Fig. 1a.

125 *i. Isotope composition of plant xylem water at stem base.*

126 The deuterium isotope composition of xylem water ( $\delta^2H_{X,0,t}$ ) of an individual plant at  
127 stem base (i.e. height zero;  $h = 0\text{m}$ ; Fig. 1a) at time  $t$ , can theoretically be derived using the  
128 multi-source mixing model approach introduced by Phillips & Gregg (2003). Considering a  
129 root zone divided into  $n$  discrete soil layers of equivalent thickness  $\Delta z$ , if the deuterium isotope  
130 composition of soil water ( $\delta^2H_{S,i}$ ) in each soil layer is constant over time, a reasonable  
131 assumption if the isotopic measurements are conducted during rain-free periods,  $\delta^2H_{X,0,t}$  can  
132 be expressed as:

$$133 \quad \delta^2H_{X,0,t} = \sum_{i=1}^n f_{i,t} \cdot \delta^2H_{S,i} \quad \text{Eq. (1)}$$

134 where  $f_{i,t}$  is the fraction of water taken up at the  $i^{\text{th}}$  soil layer (Fig. 1a) defined as:

$$135 \quad f_{i,t} = \frac{RWU_{i,t}}{\sum_{i=1}^n RWU_{i,t}} \quad \text{Eq. (2)}$$

136 and  $RWU_{i,t}$  is the net amount of water entering and leaving the roots at time  $t$  in the  $i^{\text{th}}$  soil layer  
137 ( $RWU_{i,t}$  is defined positive when entering the root). The current representation of the model  
138 assumes no water loss via the root system and no mixing of the extracted water from different  
139 soil layers within the roots until the water enters the stem base. When tree capacitance is  
140 neglected, the sum of  $RWU_{i,t}$  across the entire root zone is equal to the instantaneous sap flow  
141 at time  $t$ ,  $SF_t$ :

$$142 \quad SF_t = \sum_{i=1}^n RWU_{i,t} = \sum_{i=1}^n -k_i \cdot A_{R,i} \cdot [\Psi_{X,0,t} - (\Psi_{S,i,t} - z_i)] \quad \text{Eq. (3)}$$

143 Where  $k_i$  is the plant specific total soil-to-root conductance,  $\Psi_{X,0,t}$  is the water potential at the  
144 base of the plant stem and  $\Psi_{S,i,t}$  is the soil water matric potential (Fig. 1a). Total plant water



145 potential is generally defined as the sum of the pressure, gravity and matrix potential. Hence,  
146  $\Psi_{X,0,t}$  represents the xylem pressure potential. The term  $z_i$  is the gravimetric water potential  
147 necessary to lift the water from depth  $z_i$  to the base of the stem, assuming a hydrostatic gradient  
148 in the transporting roots. The model considers  $z_i$  to be a positive value (zero at the surface), thus  
149  $z_i$  is subtracted from  $\Psi_{S,i,t}$ .  $A_{R,i}$  is the absorptive root area distribution over soil layer  $i$  (Fig. 1a).  
150 This parameter can be derived from plant allometric relations (Čermák *et al.*, 2006) which is  
151 subsequently distributed over the different soil layers via Jackson *et al.* (1995).  
152 The total soil-to-root conductance is calculated assuming the root and soil resistances are  
153 connected in series (Fig. 1a):

$$154 \quad k_i = \frac{k_R \cdot k_S}{k_R + k_S} \quad \text{Eq. (4)}$$

155 where  $k_R$  is the effective root radial conductivity (assumed constant and uniform), and  $k_S =$   
156  $K_{S,i}/\ell$  is the conductance associated with the radial water flow between soil and root surface.  
157  $\ell = 0.53/\sqrt{\pi \cdot B_i}$  represents the effective radial pathway length of water flow between bulk soil  
158 and root surface (De Jong van Lier *et al.*, 2008)(Vogel *et al.*, 2013).  $B_i$  represents the overall  
159 root length density distribution per unit of soil.  $K_{S,i}$  is the soil hydraulic conductivity for each  
160 soil depth.  $K_{S,i}$  depends on soil water moisture and thus relates to the soil water potential  $\Psi_{S,i,t}$   
161 of the soil layer where the water is extracted.  $K_{S,i}$  is computed using the Clapp & Hornberger  
162 (1978) formulation:

$$163 \quad K_{S,i} = K_{S,max} \cdot \left( \frac{\Psi_{sat}}{\Psi_{S,i,t}} \right)^{2+\frac{3}{b}} \quad \text{Eq. (5)}$$

164 where  $K_{S,max}$  is the soil conductivity at saturation and  $b$  and  $\Psi_{sat}$  are empirical constants that  
165 depend on soil type (here considered as constant through all soil layers).

166 Subsequently,  $f_{i,t}$  can be restructured as:



$$167 \quad f_{i,t} = \frac{k_i \cdot A_{R,i} \cdot \Delta \Psi_{i,t}}{\sum_{i=1}^n k_i \cdot A_{R,i} \cdot \Delta \Psi_{i,t}} \quad \text{Eq. (6)}$$

168 where the root to soil water potential gradient is represented as  $\Delta \Psi_{i,t} = \Psi_{X,0,t} - (\Psi_{S,i,t} - z_i)$ .

169 Combining Eq. (1) and Eq. (6) then allows derivation of  $\delta^2 H_{X,0,t}$  as follows:

$$170 \quad \delta^2 H_{X,0,t} = \sum_{i=1}^n \left( \frac{k_i \cdot A_{R,i} \cdot \Delta \Psi_{i,t}}{\sum_{j=1}^n k_j \cdot A_{R,j} \cdot \Delta \Psi_{j,t}} \cdot \delta^2 H_{S,i} \right) \quad \text{Eq. (7)}$$

171 This equation requires estimates of  $\Delta \Psi_{i,t}$ , which is preferably measured instantaneously in the  
 172 field (i.e. via stem and soil psychrometers for  $\Psi_{X,0,t}$  and  $\Psi_{S,i,t}$ , respectively). However, as  
 173 measurements of  $\Psi_{X,0,t}$  are not always available, estimated  $\hat{\Psi}_{X,0,t}$  can be derived from sap flow  
 174 by re-organizing Eq. (3) into:

$$175 \quad \hat{\Psi}_{X,0,t} = \frac{\sum_{i=1}^n [k_i \cdot A_{R,i} \cdot (\Psi_{S,i,t} - z_i)] - SF_t}{\sum_{i=1}^n k_i \cdot A_{R,i}} \quad \text{Eq. (8)}$$

176 which then allows replacement of  $\Psi_{X,0,t}$  with  $\hat{\Psi}_{X,0,t}$  in Eq. (7).

177 *ii. Height-dependent isotope composition of plant xylem water*

178 In our model, from the stem base, the water isotopologues simply move upwards with  
 179 the xylem sap flow, hence diffusion and water fractionation during transportation are not  
 180 considered. The isotope composition in xylem water at height  $h$  and time  $t$  ( $\delta^2 H_{X,h,t}$ ) is then the  
 181 isotope composition of xylem water at stem base at time  $t - \tau$ .

$$182 \quad \delta^2 H_{X,h,t} = \delta^2 H_{X,0,t-\tau} \quad \text{Eq. (9)}$$

183 where  $\tau$  is the lag before  $\delta^2 H_{X,0,t}$  reaches stem height  $h$  (Fig. 1a) which depends only on the  
 184 true sap flux density in the xylem ( $SF_V$ ). True sap flux density indicates the real speed of vertical  
 185 water displacement within a plant, derived by dividing  $SF_t$  over the lumen area of the plant ( $A_x$ ;  
 186 Fig. 1a) i.e. the total cross-sectional area of the vessels.  $\tau$  was derived from the mass  
 187 conservation equality:



188 
$$h \cdot A_x = \int_{t=0}^{\tau} SF_t dt$$
 Eq. (10)

189 Note that since most scientific studies express sap flux density as the sap flow over the total  
190 sapwood area ( $SF_S$ ), rather than over the total vessel lumen area ( $SF_V$ ), for consistency, we will  
191 present the model outputs as functions of  $SF_S$ .

192 *iii. Model parameterization and analyses*

193 We adopted the basic plant parameters from Huang *et al.* (2017) for a loblolly pine  
194 (*Pinus taeda L.*) (Table S1). We started with synthetic sap flow patterns and volumes extracted  
195 from the model runs of Huang *et al.* (2017) for a typical day (day 11 of the 30 days sequence),  
196 and assumed no variation between days. Sap flow follows the plant's water demand which is  
197 the result of daily cycles of transpiration driven by photosynthetic active solar radiation (PAR),  
198 vapor pressure deficit (VPD) and optimal stomatal response (Epila *et al.*, 2017). Secondly, both  
199 the soil water potential ( $\Psi_{S,i,t}$ ) and deuterium isotope composition of soil water ( $\delta^2H_{S,i}$ )  
200 profiles with soil depth were adopted from Meißner *et al.* (2012) (Fig. S2, see Table S1 for  
201 equations) and were assumed to stay constant over time. Since measurements of Meißner *et al.*  
202 (2012) are derived from a silt loam plot in the temperate climate of central Germany, soil  
203 parameters were selected accordingly from Clapp & Hornberger (1978). Subsequently, the  
204 following model simulations were executed (see Fig.1a):

205 **1) Analysis A1: impact of temporal  $SF_t$  variation on the isotope composition of**  
206 **xylem water at a fixed stem height.** Temporal patterns in deuterium isotope  
207 composition in xylem water ( $\delta^2H_X$ ) were evaluated for a typical situation, i.e.  
208 measurement at breast height ( $h=1.30$  m), conforming to standard practice of RWU  
209 assessment.



210           2) **Analysis A2: impact of temporal  $SF_t$  variation at different tree heights.**

211           Temporal patterns in  $\delta^2H_{X,i}$  within a tree at various sampling heights (5, 10 and 15  
212           m).

213           3) **Analysis A3: impact of temporal  $SF_t$  variation on the isotope composition of**

214           **xylem water and the timing of sampling.** Representation of the profile of  $\delta^2H_X$   
215           along the full height of a tree, measured at different sampling times (9:00, 11:00 and  
216           13:00), with the standard parameterization given in Table S1.

217           4) **Analysis B: variation in  $\delta^2H_X$  due to differences in absolute daily average sap**

218           **flow speed.** Diurnal patterns in the deuterium isotope composition of xylem water  
219           in trees that differ solely in daily averaged  $SF_V$ , which are set to 0.56, 0.28 and 0.14  
220           m h<sup>-1</sup> (respectively corresponding to  $SF_S$  values of 0.08, 0.04 and 0.02 m h<sup>-1</sup>).

221           All parameters (e.g. RWU) of the four analyses are given in Table S1.

222           Model runs for each analysis were compared to a null model. The null model adopts the  
223           standard assumption of zero variation in  $\delta^2H_X$  along the length of the plant body. We used  
224           extraction protocol related measurement errors with an accepted maximum error range of 3‰  
225           when water extraction recovery rates are higher than 98% (Orlowski *et al.*, 2013). In our null  
226           model, this is represented by a normal distribution with a mean of 0‰ and a standard deviation  
227           of 1‰, i.e.  $N(\mu=0‰, \sigma=1‰)$ , which makes the probability of an error of  $\geq 3‰$  highly unlikely  
228           ( $p \leq 0.0027$ ). Analytical errors introduced by the measurement device, i.e. a Picarro (California,  
229           USA), are considered negligible relative to the extraction error. Note that  $SF_V$ , which  
230           normalizes sap flow over total vessel lumen area, is correlated with plant diameter at breast  
231           height (DBH) which enables comparison with field measurements without the need for explicit  
232           consideration of DBH in the model. SWIFT was implemented in R version 3.4.0 (R Core Team,  
233           2017), and is publicly available (see GitHub repository HannesDeDeurwaerder/SWIFT).

234



235 **2.1.2. Estimation of rooting depth**

236 RWU depths were derived from the simulated  $\delta^2H_X$  values by use of both the direct inference  
237 method and the end-member mixing analysis method, together representing 96% of the applied  
238 methods in literature (Rothfuss & Javaux, 2017). We refer readers to Rothfuss & Javaux (2017)  
239 for a complete discussion of these techniques. Here, average rooting depth is assumed to be the  
240 depth obtained by relating the simulated  $\delta^2H_X$  with the  $\delta^2H_{S,i}$  depth profile. We compared  
241 rooting depth estimates from simulated  $\delta^2H_X$ , as described in the analyses above, with the true  
242 average rooting depth. The true average rooting depth was defined as the depth corresponding  
243 to the daily weighted average  $\delta^2H_X$ , calculated as the weighted sum of  $\delta^2H_{X,i,t}$  and the relative  
244 fraction of water taken up at each depth.

245

246 **2.1.3. Sensitivity analysis**

247 We performed two sensitivity analyses to assess the relative importance of all parameters in  
248 generating variance in  $\delta^2H_X$  along the length of a plant. In both sensitivity analyses, we varied  
249 model parameters one-at-the-time to assess the local sensitivity of the model outputs. The  
250 sensitivity analysis provides insight into the design of field protocols, revealing potential key  
251 measurements in addition to any caveats.

252 We first assessed model sensitivity to (bio)physical variables by modifying model  
253 parameters of soil type, sap flow and root properties as compared to the standard  
254 parameterization (given in Table S1). The following sensitivity analyses were considered:

255 **Soil type:** The soil moisture content over all soil layers ( $\theta_{S,i,t}$ ) can be deduced from the  
256 considered Meißner et al. (2012)  $\Psi_{S,i,t}$  profile (see Fig. S2 and Table S1) using the Clapp  
257 & Hornberger (1978) equation:



$$\theta_{S,i,t} = \theta_{sat} \cdot \left( \frac{\Psi_{S,i,t}}{\Psi_{sat}} \right)^{-1/b} \quad \text{Eq. (11)}$$

258  
259 Where  $\theta_{sat}$ ,  $\Psi_{sat}$  and  $b$  are soil-type specific empirical constants that correspond to  
260 sandy loam soil textures in the standard model parameterization (Clapp & Hornberger,  
261 1978). The derived soil moisture profile ( $\theta_{S,i,t}$ ), in turn, then provides a basis to study  
262 the impact of other soil textures. A new soil texture specific  $\Psi_{S,i,t}$  profile can then be  
263 deduced by using  $\theta_{sat}$ ,  $\Psi_{sat}$  and  $b$  values corresponding to different soil texture types  
264 (values from Table 2 of Clapp & Hornberger (1978)). This enabled us to study  $\Psi_{S,i,t}$   
265 profiles for four distinct soil types, i.e. (i) sand, (ii) loam, (iii) sandy clay and (iv) clay  
266 soils, in relation with the original silt loam  $\Psi_{S,i,t}$  profile.

267 **Volume of water uptake:** We varied the total diurnal volume of water taken up by the  
268 tree. New  $SF_t$  values are scaled using algorithms from literature that provide an estimate  
269 of the daily sap flow volume of a tree based on its DBH (Andrade *et al.*, 2005; Cristiano  
270 *et al.*, 2015).

271 **Root conductivity:** We varied the root membrane permeability ( $k_R$ ) to match multiple  
272 species specific values found in literature (Sands *et al.*, 1982; Rüdinger *et al.*, 1994;  
273 Steudle & Meshcheryakov, 1996; Leuschner *et al.*, 2004).

274 The second set of sensitivity analyses test the impact of root hydraulics, sap flux density  
275 and sampling strategies on the sampled  $\delta^2H_x$ . We obtained 1000 samples per parameter from  
276 corresponding distributions and ranges (given in Table S2) with a Latin hypercube approach  
277 (McKay *et al.*, 1979; McKay, 1988). This is a stratified sampling procedure for Monte Carlo  
278 simulation that can efficiently explore multi-dimensional parameter space. In brief, Latin  
279 Hypercube sampling partitions the input distributions into a predefined number of intervals  
280 (here 1000) with equal probability. Subsequently, a single sample per interval is extracted in an



281 effort to evenly distribute sampling effort across all input values and hence reduce the number  
282 of samples needed to accurately represent the parameter space.

283

## 284 **2.2. Part B: Empirical exploration**

### 285 **2.2.1. Data on variation in i-H<sub>2</sub>O-xyl with plant height**

286 We used data for six canopy trees and six canopy lianas sampled on two subsequent dry days  
287 (24-25 August, 2017) at the Laussat Conservation Area in Northwestern French Guiana. The  
288 sampling site (05°28.604'N-053°34.250'W) lies approximately 20 km inland at an elevation of  
289 30 m a.s.l. This lowland rainforest site has an average yearly precipitation of 2500 mm yr<sup>-1</sup>  
290 (Baraloto *et al.*, 2011). Average and maximum daily temperatures of respectively 30°C and  
291 36°C were measured during the sampling period. Sampled individuals are located in the white  
292 sands forest habitat (Baraloto *et al.*, 2011), on a white sandy ultisol with typically high  
293 percentage of sand.

294 Individuals (Table 2) were selected based on assessment of climbable tree, intactness of  
295 leafy canopy vegetation and close vicinity with one another to optimize similarity in  
296 meteorological and edaphic characteristics. Liana diameters were measured at 1.3 m from the  
297 last rooting point (Gerwing *et al.*, 2006), tree diameters were measured at 1.3 m (Table 2).  
298 Sampling was performed between 9am and 2pm to assure high sap flow. Liana and tree  
299 sampling allowed highly contrasted sap flux density (Gartner *et al.*, 1990).

300

### 301 **2.2.2. Sampling strategy**

302 The stem xylem tissue of individual plants was sampled at different heights (1.3, 5, 10, 15 and  
303 20 m where possible) at the same radial position of the stem, between 8:00 and 15:00. The order  
304 of sampling, i.e. ascending versus descending heights, was randomized. Tree stem xylem



305 samples were collected with an increment borer (5 mm diameter), resulting in wooden cylinders  
306 from which bark and phloem tissues were removed. Coring was performed within the horizontal  
307 plane at the predefined heights, oblique to the center of the stem to maximize xylem and  
308 minimize heartwood sampling, and slowly to avoid heating up the drill head and kinetic  
309 fractionation. Taking one sample generally took between 5 and 10 minutes. Since coring lianas  
310 was not possible, we collected cross-sections of the lianas after removing the bark and phloem  
311 tissue with a knife. All materials were thoroughly cleaned between sampling using a dry cloth  
312 to avoid cross-contamination. Upon collection, all samples were placed in pre-weighed glass  
313 collection vials, using tweezers, to reduce contamination of the sample. Glass vials were  
314 immediately sealed with a cap and placed in a cooling box, to avoid water loss during  
315 transportation.

316

### 317 **2.2.3. Sample processing**

318 Sample processing was performed as in De Deurwaerder *et al.* (2018). Specifically, all fresh  
319 samples were weighed, transported in a cooler and frozen before cryogenic vacuum distillation  
320 (CVD). Water was extracted from the samples via CVD (4 h at 105°C). Water recovery rates  
321 were calculated from the fresh weight, weight after extraction and oven dry weight (48 h at  
322 105°C). Samples were removed from the analysis whenever weight loss resulting from the  
323 extraction process was below 98% (after Araguás-Araguás *et al.*, 1998). The isotope  
324 composition of the water in the samples was measured by a Wavelength-Scanned-Cavity Ring-  
325 Down Spectrometer (WS-CRDS, L2120-i, Picarro, California, USA) coupled with a vaporizing  
326 module (A0211 High Precision Vaporizer) through a micro combustion module to avoid  
327 organic contamination (Martin-Gomez *et al.*, 2015; Evaristo *et al.*, 2016). Internal laboratory  
328 references were used for calibration, with measurement precision of  $\pm 0.1\%$  and  $\pm 0.3\%$  for  $\delta^{18}\text{O}$



329 and  $\delta^2\text{H}$ , respectively. Post-processing was performed using SICalib (version 2.16; Gröning,  
330 2011)

331 Isotopic composition, expressed in terms of  $[^{18}\text{O}]/[^{16}\text{O}]$  and  $[^2\text{H}]/[^1\text{H}]$  ratios, is  
332 represented by  $\delta$ -values (in our case,  $\delta^{18}\text{O}$  and  $\delta^2\text{H}$ ), which indicate the deviation from a  
333 designated standard (i.e. V-SMOW, Vienna Standard Mean Ocean Water) in parts per thousand  
334 (expressed in ‰):

$$335 \quad \delta_{\text{sample}(\text{‰})} = \left( \frac{R_{\text{sample}}}{R_{\text{standard}}} - 1 \right) \cdot 1000 \quad \text{Eq. (12)}$$

336 where  $R$  is the heavy to light isotope ratio measured in the sample or standard. We calculate  
337 normalized  $i\text{-H}_2\text{O}\text{-}xyl$  for each individual at every sampled height  $h$  ( $\varepsilon^2H_X$  and  $\varepsilon^{18}O_X$ ) as being  
338 the deviation of each sample from the stem mean (derived from all stem samples of that  
339 individual):

$$340 \quad \varepsilon^2H_{X,h} = \delta^2H_{X,h} - \frac{1}{N} \sum_{h=1}^N \delta^2H_{X,h} \quad \text{Eq. (13)}$$

341 with  $N$  the number of heights sampled per individual.

342

#### 343 **2.2.4. Data on high temporal-resolution variation in $i\text{-H}_2\text{O}\text{-}xyl$**

344 We used data from three extensive field campaigns by Zhao *et al.* (2014) who sampled plant  $i\text{-}$   
345  $\text{H}_2\text{O}\text{-}xyl$  at high temporal resolution in the Heihe River Basin (HRB), northwestern China. Four  
346 distinct study locations differing in altitude, climatological conditions and ecosystem types  
347 were selected. At each location, the dominant tree, shrub and/or herb species was considered  
348 for sampling. In August 2009, *Populus euphratica* was sampled in the Qidaoqiao riparian forest  
349 ( $42^\circ 01' \text{N}$ - $101^\circ 14' \text{E}$ ) and *Reaumuria soongorica* in the Gobi desert ecosystem ( $42^\circ 16' \text{N}$ -  
350  $101^\circ 17' \text{E}$ ; 906-930 m a.s.l). In June–September 2011 *Picea crassifolia*, *Potentilla fruticosa*,  
351 *Polygonum viviparum* and *Stipa capillata* were measured in the Pailugou forest ecosystem  
352 ( $38^\circ 33' \text{N}$ - $100^\circ 18' \text{E}$ ; 2700-2900 m a.s.l). All species were samples 2-hourly, with the exception



353 of *P. crassifolia* which was measured hourly. Stem samples were collected for trees and shrubs,  
354 while root samples were obtained for the herb species (more details in Zhao *et al.* (2014)).

355 Upon collection, all samples were placed in 8 mL collection bottles and frozen in the  
356 field stations before transportation to the laboratory for water extraction via CVD (Zhao *et al.*,  
357 2011). Both  $\delta^{18}O$  and  $\delta^2H$  were assessed with an Euro EA3000 element analyzer (Eurovector,  
358 Milan, Italy) coupled to an Isoprime isotope ratio mass spectrometer (Isoprime Ltd, UK) at the  
359 Heihe Key Laboratory of Ecohydrology and River Basin Science, Cold and Arid Regions  
360 Environmental and Engineering Research institute. Internal laboratory references were used for  
361 calibration, resulting in measurement precision of  $\pm 0.2\%$  and  $\pm 1.0\%$  for  $\delta^{18}O$  and  $\delta^2H$ ,  
362 respectively.

363

### 364 **3. Results**

#### 365 **3.1. Part A: Modelling exploration**

##### 366 **3.1.1. Simulated temporal fluctuation in isotope composition of plant xylem water**

###### 367 *i. Isotope composition of xylem water at stem base and basic model behavior*

368 At the stem base, simulated  $\delta^2H_{X,0,t}$  displays a diurnal fluctuation (Fig. 2) that corresponds to  
369 the daily sap flow pattern (Fig. 2c). This pattern is caused by shifting diurnal RWU depth. Early  
370 in the morning, when transpiration is low, most of the RWU occurs in deeper layers, where soil  
371 water potential is less negative and isotopic composition of soil water is dominated by depleted  
372 deuterium (Fig. S2a-b). As transpiration increases during the day, a significant proportion of  
373 RWU is extracted from the drier shallow layers, which have an enriched isotopic composition.  
374 In the afternoon, as transpiration declines, isotopic composition reflects again the composition  
375 of the depleted deep soil and it remains constant throughout the night because SWIFT does not  
376 consider mixing of the internal water in stem and roots nor hydraulic lift.



377 The most enriched  $\delta^2H_X$ -values (approx. -59‰) are found in alignment with the diurnal  
378 minimum of  $\Psi_{X,0,t}$  (approx. -0.85 MPa, Fig. 2c). At this moment,  $\Delta\Psi_{i,t}$  are maximized, enabling  
379 water extracting from the upper and driest soil layers. Most root biomass is located near the  
380 surface (cf. Jackson *et al.*, 1995; Fig. S2c) and uptake in these layers will result in relatively  
381 high contributions to the total RWU.

382 In contrast,  $\Delta\Psi_{i,t}$  are smaller in the early morning and late afternoon causing root water  
383 uptake in the upper soil layers to halt. The decreasing  $\Delta\Psi_{i,t}$  translates into higher proportions of  
384 RWU originating from deeper, more depleted soil layers. This causes  $\delta^2H_X$  to drop to a baseline  
385 of approx. -67‰. This afternoon depletion of  $\delta^2H_X$  will henceforth be indicated as the  $\delta^2H_X$ -  
386 baseline drop.

387 *ii. Isotope composition of xylem water at different times, heights and SFv*

388 Temporal fluctuation in  $\delta^2H_X$  within a tree at 1.3 m (i.e. the standard sampling height;  
389 Analysis A1; Fig. 1a) and at other potential sampling heights (e.g. branch collection; Analysis  
390 A2; Fig. 1a), are provided in Fig. 2a-b, respectively. Both analyses show that fluctuations in  
391  $\delta^2H_X$  depend on the height of measurement and the corresponding time needed to move the  
392 water along the xylem conduits. Note that it depends on the selected temporal resolution  
393 whether the  $\delta^2H_X$ -baseline drop at a given height equals the (stem base) minimum (here 1 min,  
394 see Fig. S6). The relation between  $\delta^2H_X$  variance and cumulative sap flow volumes is provided  
395 in Fig. 2d. Here, the piston flow dynamics in SWIFT originate from lateral translation of the  
396  $\delta^2H_X$  fluctuation at  $\delta^2H_{X,0,t}$ . In addition to sampling height, analysis A3 depicts the importance  
397 of sampling time (Fig. 1b).

398 Analysis B outputs predict the occurrence and width of the  $\delta^2H_X$ -baseline drop as a function  
399 of  $SF_V$  (Fig. 1c). Moreover, depending on  $SF_V$ , the isotopic signal can take hours or days to  
400 travel from roots to leaves - as is also observed experimentally (Steppe *et al.*, 2010). Low  $SF_V$



401 allows multiple  $\delta^2H_X$ -baseline drops over the length of a single tree. This means that sampled  
402  $\delta^2H_X$  can reflect soil isotopic composition of the past several days. This has direct implications  
403 for comparing samples obtained at different times and heights and for species that experienced  
404 different  $SF_V$  histories.

405

### 406 **3.1.2. Potential biases in root depth estimation**

407 Both timing of measurement (Fig. 3a) and  $SF_V$  (Fig. 3b) influence rooting depth estimates  
408 derived via the direct inference and end-member mixing analysis method (Fig. S2) (Rothfuss  
409 & Javaux, 2017). Collection of tree samples at 1.30 m can result in erroneous estimation,  
410 deviating up to 104% from the average daily RWU depth (Fig. 3). Plotting the relative error in  
411 RWU depth as a function of time and  $SF_V$  (Fig. 3c) shows that it is possible to time  $\delta^2H_X$   
412 measurements in a fashion that captures unbiased estimates of the average RWU depth. Xylem  
413 water sampling should be timed to capture the  $\delta^2H_X$  that corresponds to water extracted at peak  
414 RWU, and the expected sampling time can be derived by considering the time needed for the  
415 water to reach the point of measurement (i.e. at 1.30 m in Fig. 3). In general, SWIFT predicts  
416 that plants with slow  $SF_V$  should not be measured during the morning hours, as this results in  
417 measuring the preceding days' absorbed water. In contrast, trees with higher  $SF_V$  support earlier  
418 sample collection.

419

### 420 **3.1.3. Sensitivity analysis**

421 Our sensitivity analyses shows that the expected absolute error in RWU depth assessment is  
422 directly related to both 1) maximum variance in and 2) the probability of sampling non-  
423 representative  $\delta^2H_X$  values. The maximum variance depends on the height, while the probability  
424 of sampling non-representative areas depends on the width of the “ $\delta^2H_X$ -baseline drop”



425 respectively (defined above). Hence, bias in  $\delta^2H_X$  is predominantly a function of the sampling  
426 strategy (timing and height of sampling; Fig. S3) in relation to the  $SF_V$  of the plant (shown by  
427 a strong effect of lumen area and total diurnal RWU volume in Fig. S3) and some biophysical  
428 parameter (Fig. S4). We summarized the most important variables as predicted by SWIFT, that  
429 should be considering in RWU studies below.

430 Plants on loam soils show larger diurnal  $\delta^2H_X$  variances ( $\sim 8\%$ ) in comparison with those of  
431 clay soils ( $\sim 3\%$ ). Larger variances correspond to potentially larger error, but the steeper slope  
432 of the  $\delta^2H_X$  curve results in a thinner  $\delta^2H_X$ -baseline drop. Hence, loam soil can result in  
433 potentially the largest errors but this is mediated by a lower probability of sampling non-  
434 representative  $\delta^2H_X$  values during the day.

435 The volume of water taken up by the plant ( $SF_t$ ; Fig. S4b) affects xylem water potential of  
436 the plant at stem base ( $\Psi_{X,0,t}$ ). Higher  $SF_t$  requires more negative  $\Psi_{X,0,t}$ , enabling the plant to  
437 access more shallow and enriched soil layers. Therefore, an increase in  $SF_t$  results in the  
438 increase of maximum  $\delta^2H_X$  values (increased maximum error) but also results in a smaller width  
439 of the baseline drop (Fig. 1c). Lower  $SF_t$  result in smaller error, but larger probability of  
440 sampling an non-representative area (Fig. 1c).

441 Root properties, i.e. root membrane permeability (Fig. S4c) strongly influence both the total  
442 range of  $\delta^2H_X$  variance and the width of the  $\delta^2H_X$ -baseline drops. Decreasing root permeability  
443 results in thinner  $\delta^2H_X$ -baseline drops, but higher maximum  $\delta^2H_X$  variance.

444

### 445 **3.2. Part B: Empirical exploration**

446 The observed normalized deuterium isotope composition in xylem water ( $\varepsilon^2H_X$ ) along the height  
447 of lianas and trees showed strong intra-individual variance exceeding the null model by a factor



448 of 3.2 and 4.3 respectively (Fig. 4a-b). Specifically, differences up to 13.1‰ and 18.3‰ in  $\delta^2H$   
449 and 1.3‰ and 2.2‰ in  $\delta^{18}O$  are observed as intra-individual variances for trees and lianas  
450 respectively (Table 2).

451 Similarly, excessive diurnal intra-individual  $\delta^2H_X$  variances emerge in all considered  
452 growth forms (Fig. 5). Observed maximums were 18.0‰, 21.0‰ and 25.2‰ in  $\delta^2H_X$  for trees,  
453 shrubs and herbs respectively (Fig. 5; 2.8‰, 6.8‰ and 6.5‰ in  $\delta^{18}O_X$  in Fig. S5). The null  
454 model expected diurnal variance was exceeded for each species during its measurement period,  
455 with the exception of  $\delta^2H_X$  measurements of *P. euphratica*. The latter is a riparian forest species,  
456 living along the river course, where an easily accessible and abundant ground-water reservoir  
457 drives its RWU and *i-H<sub>2</sub>O-xyl*.

458

## 459 **4. Discussion**

### 460 **4.1. Dynamic diurnal isotope compositions of xylem water along plant stems**

461 Our model shows that basic plant hydraulic functioning will result in shifting mixtures of  $\delta^2H_X$   
462 entering the plant (Fig. 1a-2a). Daily  $\Psi_{X,0,t}$  fluctuations interact with the  $\Psi_{S,i,t}$  profile causing  
463 different parts of the root distribution to be active during the day. The fluctuations in  $\delta^2H_X$  at  
464 the stem base propagate along the xylem with a velocity proportional to the sap flow and this  
465 produces variability in sampled  $\delta^2H_X$  that is much larger than the expected measuring error. In  
466 addition, empirical field data show excessive *i-H<sub>2</sub>O-xyl* variance along the stem length (Fig. 4)  
467 and over a short time frame (i.e. sub-daily, Fig. 5). Therefore, the assumption of uniform  $\delta^2H_X$   
468 along the length of a lignified plant is rejected, both theoretically and empirically.  
469 Consequently, rather than being static,  $\delta^2H_X$  values along the height of a plant should be  
470 considered a dynamic diurnal process.



471           Importantly, we show that violation of this assumption results in incorrect assessment  
472 of differences in RWU depths between plants. Differences do not necessarily result from  
473 variability in RWU depth, but may result from monitoring plants at different heights (Fig. 2),  
474 at different times (Fig. 1b) or by comparing individuals which have different  $SF_V$  (Fig. 1c). Our  
475 sensitivity analysis reveals that various soil and plant characteristics have an important role in  
476 determining both the daily maximum  $\delta^2H_X$  variance as well as the width of the  $\delta^2H_X$  -baseline  
477 drop. These two characteristics directly impact (i) the expected maximum bias in estimates of  
478 RWU depth and (ii) the chance of measuring  $\delta^2H_X$  values that do not represent a mixture of all  
479 rooting layers during peak RWU (i.e. the baseline drop). Our work supplements the recent  
480 overview of Penna *et al.* (2018) discussing challenges in using stable isotope composition of  
481 water to study the terrestrial water fluxes. We additionally advocate that future research should  
482 explore the minimum set of (bio)physiological drivers and processes that require quantification  
483 to correctly interpret  $\delta^2H_X$  along the length of a plant.

484

#### 485 **4.2. General applicability of model and results**

486 A necessary condition for diurnal shifts in RWU is the existence of a water potential  
487 heterogeneity, e.g. more negative water potentials in the upper layers where trees usually have  
488 higher root density, which causes a disproportional partitioning of diurnal RWU between deep  
489 and shallow roots. Since such a gradient is formed when the upper soil layers undergo  
490 evaporation, these conditions are also necessary for the existence of a soil isotopic gradient.  
491 Thus, the problem we have identified is intrinsic to the isotopic tracing method for RWU  
492 assessment.

493           Plant transpiration results from complex interaction between atmospheric demands (i.e.  
494 driven by VPD and radiation) and stomatal conductance which depends on tolerance of drought



495 stress and soil moisture content. We may expect diurnal fluctuation in radiation and VPD, and  
496 hence in water transport and depth of water absorption, as modelled here to be a general  
497 phenomenon in nature. Hence, there is a real risk of misinterpretation and calculation errors  
498 within the existing literature whenever *i-H<sub>2</sub>O-xyl* are used to assess RWU and water competition  
499 strategies. Moreover, much greater fluctuations in VPD and radiation should be expected under  
500 natural conditions than the diurnal cycle described here, and these will increase variability of  
501 transpiration fluxes, leading to even more complex dynamics of  $\Psi_{X,0,t}$ . For instance, slight  
502 alterations in these variables, i.e. a changing degree in cloud cover, can influence  $\Psi_{X,0,t}$  rather  
503 abruptly (for e.g. Ilianas; Chen *et al.*, 2015) and lead to instantaneous changes in  $\delta^2H_X$ . Clearly  
504 this further complicates the comparison of samples from different plants and sampled at  
505 different heights and times, to date overlooked in RWU assessments, and our model certainly  
506 illustrates that these considerations are non-trivial.

507 Note that, based on our model, we expect that soil isotopic enrichment experiments will  
508 generate extensive  $\delta^2H_X$  variation along the length of trees whenever diurnal RWU fluctuations  
509 cause water extraction to shift between labeled and unlabeled soil layers. Furthermore, when  
510 enrichment experiments target trees with different hydraulic properties (such as  $SF_V$ ) care  
511 should be taken as to determine when and where to sample these trees in order to assess an  
512 enriched isotope composition. Researchers should be certain the signal will be present at the  
513 sample height (Fig. 1-2).

514

#### 515 **4.3. Alternative causes of *i-H<sub>2</sub>O-xyl* fluctuation.**

516 The SWIFT model provides a simple traceable and mechanistic explanation, using diurnal  
517 variations in  $SF_i$  and RWU, for the excessive variance and dynamic nature of the *i-H<sub>2</sub>O-xyl*  
518 fluctuations with plant height and time of field samples (e.g. Fig. 4-5) and elsewhere (Cooper



519 *et al.* 1991). We believe that our model provides a plausible simple explanation for diurnal *i*-  
520  $H_2O$ -*xyl* variation, which contributes to the variation that is observed empirically. Nevertheless,  
521 the model necessarily represents a simplified representation of plant hydraulic functioning and  
522 is therefore limited. There may be alternative causes that contribute to the observed intra-  
523 individual *i*- $H_2O$ -*xyl* variances. We discuss these here.

524 *i. Fractionation at root level*

525 An increasing body of observations show the occurrence of isotopic fractionation at the root  
526 level governed by root membrane transport (Lin & Sternberg, 1993; Vargas *et al.*, 2017) or by  
527 unknown reasons (Zhao *et al.*, 2016). Brinkmann *et al.* (2019) hypothesize that root level  
528 fractionation causes disparity when RWU depth calculations based on  $\delta^2H_X$  measurements are  
529 compared with those of  $\delta^{18}O_X$ . However, it is difficult to imagine a scenario where root  
530 fractionation by itself can explain the observed diurnal fluctuations in *i*- $H_2O$ -*xyl* with height  
531 and time. Even if root fractionation significantly contributed to variation in *i*- $H_2O$ -*xyl*, we would  
532 still need to take into account diurnal fluctuation in RWU to explain the observed patterns.

533 *ii. Temporal and spatial soil dynamics*

534 The dynamics of soil water movement is complex and soil water content can be extremely  
535 heterogeneous in the three spatial dimensions and such variation is currently not represented in  
536 SWIFT. Hydraulic lift is a process that generates a vertical redistribution of water in the soil  
537 through the roots (Dawson & Ehleringer, 1993), which may change the soil water isotopic  
538 composition and mixture drawn up by roots. However, hydraulic lift should redistribute and  
539 mix the depleted isotopic signal of deeper layers with the enriched signal of shallower layers.  
540 This should lead to lower variation in the soil profile, and less variation along plant length, as  
541 such hydraulic lift cannot explain the observed patterns. Heterogeneity in horizontal  
542 distribution of water pockets may also affect *i*- $H_2O$ -*xyl* variance. Under these conditions, the



543 horizontal distribution of the absorptive root area becomes more important. However, as the  
544  $\Psi_{S,i,t}$  and the isotope composition of soil water of these pockets are interlinked, the mechanistic  
545 driver of water extraction is the diurnal fluctuation in water potential gradients in the plant,  
546 conform SWIFT.

547 *iii. Storage tissue and phloem enrichment*

548 Storage tissues release water and sugars in the xylem conduits on a daily basis to support  
549 water transpiration demand (Goldstein et al., 1998; Morris et al., 2016; Secchi et al., 2017) or  
550 to repair embolism (Salleo et al., 2009; Secchi et al., 2017). Both water and sugars are  
551 transported in and out storage tissue via symplastic pathways using plasmodesmata and  
552 aquaporins (Knipfer et al., 2016; Secchi et al., 2017), a pathway which has been linked to  
553 isotopic fractionation in roots (Ellsworth & Williams, 2007). Moreover, phloem transports  
554 photosynthetic assimilates constructed at the leaf level potentially affected by transpiration  
555 fractionation (Gessler *et al.*, 2013). Hence, these metabolic molecules might be constructed  
556 from enriched  $^2H$  and  $^{18}O$  atoms. Water release from storage or phloem tissue might locally  
557 alter *i-H<sub>2</sub>O-xyl* (White et al., 1985). Additionally, time between water storage and release could  
558 bridge multiple days, and corresponding isotopic composition may reflect different soil  
559 conditions. It is evident that such dynamics are complex, and it is hard to predict how storage  
560 tissue and phloem enrichment affect the *i-H<sub>2</sub>O-xyl* patterns observed here. Xylem isotopic  
561 sampling cannot differentiate between water resulting from RWU or storage, and therefore we  
562 cannot discount the possibility that tissue and phloem enrichment play a role. At a minimum  
563 this adds further uncertainty to RWU assessment.

564 Further studies should determine whether the implementation of additional mechanisms  
565 such as tree capacitance, root and stem level fractionation, spatiotemporal soil water dynamics,



566 more detailed root systems or storage tissues impact the intra-individual  $i\text{-H}_2\text{O}\text{-xyl}$  and should  
567 be accounted for to improve RWU assessment and interpretation.

568

#### 569 **4.4. The way forward**

570 Combining a plant hydraulic model with *in situ*  $SF_V$  and *in situ*  $\Psi_{S,i,t}$  can help improve  
571 the robustness of RWU assessment and interpretation. Measurements of  $\Psi_{S,i,t}$  at multiple  
572 depths, i.e. by installing multiple soil water potential sensors that measure at high temporal  
573 frequency, should be especially valuable since the SWIFT model showed high sensitivity to  
574 alterations of this variable and these can be directly supplied as model inputs. At the same time,  
575 the availability of  $SF_t$  measurements allows for identifying the moment when water uptake from  
576 all root layers is at its maximum, which can be used to determine the optimal timing of sampling  
577 at a given height providing a more robust estimation of RWU depth and uptake.

578 Alongside the modeling and theoretical approach presented here, new ways to study  
579  $\delta^2H_X$  at a high temporal scale are strongly encouraged. For example, pioneering work of  
580 Volkmann *et al.* (2016) to the development of an *in situ* continuous isotope measurement  
581 technique that offers the possibility for monitoring  $i\text{-H}_2\text{O}\text{-xyl}$  at a sub hourly resolution. This  
582 technique holds strong promise for further elucidating the natural  $\delta^2H_X$  variances found within  
583 plants and the physiology processes from which these variances result. Such high temporal  
584 resolution of isotope measurements, coupled with *in situ* monitoring of various environmental  
585 and plant biophysical metrics, are needed for both model improvement and further validation.  
586 Moreover, these seem inevitable to eventually differentiate all causal mechanisms of the  
587 observed intra-individual  $i\text{-H}_2\text{O}\text{-xyl}$  variance.

588

## 589 **5. Conclusions**



590 We have demonstrated that the assumption of no intra-individual *i-H<sub>2</sub>O-xyl* variation is rapidly  
591 violated once models incorporate even basic plant hydraulic functioning. Moreover, the  
592 incorrectness of this assumption is confirmed by empirical field data, showing excessive  
593 variance and high temporal fluctuations in *i-H<sub>2</sub>O-xyl*. We expect the observed *i-H<sub>2</sub>O-xyl*  
594 variance and sub-daily fluctuations result, in part, from the mechanisms considered in the  
595 SWIFT model, though they likely represent an end product of various physiological processes  
596 which impact *i-H<sub>2</sub>O-xyl*.

597 Our theoretical explorations warn that variability in the isotope composition of plant  
598 xylem water can result in erroneous RWU depth estimation and will complicate the  
599 interpretation and comparison of data: samples taken at different heights, times or plants  
600 differing in  $SF_V$  may incorrectly show differences in RWU depth. We further predict that  
601 various soil parameters and plant hydraulic parameters affect (i) the absolute size of the error  
602 and (ii) the probability of measuring *i-H<sub>2</sub>O-xyl* values that do not represent the well-mixed  
603 values during the plants' peak RWU. Hydraulic models, such as SWIFT, should be used to  
604 design more robust sampling regimes that enable improved comparisons between studied  
605 plants. We advocate the addition of  $SF_t$ , which indirectly reflects diurnal RWU fluctuations,  
606 and  $\Psi_{S,i,t}$  monitoring as a minimum in future RWU assessments since these parameters were  
607 predicted to be the predominant factors introducing variance in *i-H<sub>2</sub>O-xyl* from the SWIFT  
608 model exploration. However, soil texture and root permeability are also key considerations to  
609 measure especially when comparing across species and sites.

610 Our findings do not exclude additional factors that impact the observed intra-individual  
611 *i-H<sub>2</sub>O-xyl* variance and temporal fluctuation. Therefore, we strongly emphasize the need for  
612 more testing. Directed studies that validate and quantify the relative impact of other plant  
613 physiological processes towards variance in *i-H<sub>2</sub>O-xyl* are a prerequisite before improved  
614 modeling tools can be developed, and bias in RWU assessments eliminated.



615 **Acknowledgement**

616 This research was funded by the European Research Council Starting Grant 637643  
617 (TREECLIMBERS), the FWO grants (1507818N, V401018N to HDD), the Carbon Mitigation  
618 Initiative at Princeton University (MD, MDV), Agence Nationale de la Recherche  
619 “Investissement d’Avenir” grant (CEBA: ANR-10-LABX-25-01), the Belgian American  
620 Educational Foundation (BAEF to FM) and the WBI (FM). We are grateful to Samuel Bodé,  
621 Megan Bartlett, Isabel Martinez Cano and Pedro Hervé-Fernández who provided feedback on  
622 analytical and interpretative aspects of the study. We thank Dries Van Der Heyden, Wim Van  
623 Nunen, Laurence Stalmans, Oscar Vercleyen, Katja Van Nieuland, Stijn Vandevoorde and  
624 Clément Stahl for data collection and lab processing. We credit Pascal Petronelli and Bruce  
625 Hoffman for species identification, and Cora N. Betsinger for proofreading. Cheng-Wei  
626 Huang’s work provided inspiration for this research.

627

628 **Author contribution**

629 H.V., M.D.V and P.B. supervised and provided guidance throughout all aspects of the research.  
630 H.D.D., M.D.V and H.V. designed the study. H.D.D., L.Z. and L.W. collected the samples and  
631 data during the field campaign and performed the processing and analysis of the samples. The  
632 model was developed and coded by H.D.D, M.D.V, M.D. and F.M. All authors contributed to  
633 interpretation of the results and to the text of the manuscript.

634

635 **Data availability**

636 Both the data and the SWIFT model are available on the GitHub repository  
637 HannesDeDeurwaerder/SWIFT

638



639 **Competing interests**

640 The authors declare that they have no conflict of interest.

641



642 **References**

- 643 **Andrade JL, Meinzer FC, Goldstein G, Schnitzer SA. 2005.** Water uptake and transport in  
644 lianas and co-occurring trees of a seasonally dry tropical forest. *Trees* **19**: 282–289.
- 645 **Araguás-Araguás L, Froehlich K, Rozanski K. 1998.** Stable isotope composition of  
646 precipitation over southeast Asia. *Journal of Geophysical Research: Atmospheres* **103**:  
647 28721–28742.
- 648 **Baraloto C, Rabaud S, Molto Q, Blanc L, Fortunel C, Herault B, Davila N, Mesones I,**  
649 **Rios M, Valderrama E. 2011.** Disentangling stand and environmental correlates of  
650 aboveground biomass in Amazonian forests. *Global Change Biology* **17**: 2677–2688.
- 651 **Brinkmann N, Eugster W, Buchmann N, Kahmen A. 2019.** Species-specific differences in  
652 water uptake depth of mature temperate trees vary with water availability in the soil. *Plant*  
653 *Biology* **21**: 71–81.
- 654 **Čermák J, Ulrich R, Staněk Z, Koller J, Aubrecht L. 2006.** Electrical measurement of tree  
655 root absorbing surfaces by the earth impedance method: 2. Verification based on allometric  
656 relationships and root severing experiments. *Tree physiology* **26**: 1113–1121.
- 657 **Cernusak LA, Farquhar GD, Pate JS. 2005.** Environmental and physiological controls over  
658 oxygen and carbon isotope composition of Tasmanian blue gum, *Eucalyptus globulus*. *Tree*  
659 *physiology* **25**: 129–146.
- 660 **Chen Y, Cao K, Schnitzer SA, Fan Z, Zhang J, Bongers F, Chen Y. 2015.** Water-use  
661 advantage for lianas over trees in tropical seasonal forests. : 128–136.
- 662 **Clapp RB, Hornberger GM. 1978.** Empirical equations for some soil hydraulic properties.  
663 *Water resources research* **14**: 601–604.
- 664 **Cooper LW, DeNiro MJ, Keeley JE. 1991.** The relationship between stable oxygen and



- 665 hydrogen isotope ratios of water in stomatal plants.
- 666 **Cristiano PM, Campanello PI, Bucci SJ, Rodriguez SA, Lezcano OA, Scholz FG,**  
667 **Madanes N, Di Francescantonio D, Carrasco LO, Zhang Y-J. 2015.** Evapotranspiration of  
668 subtropical forests and tree plantations: A comparative analysis at different temporal and  
669 spatial scales. *Agricultural and Forest Meteorology* **203**: 96–106.
- 670 **Dawson TE, Ehleringer JR. 1991.** Streamside trees that do not use stream water. *Nature*  
671 **350**: 335–337.
- 672 **Dawson TE, Ehleringer JR. 1993.** Isotopic enrichment of water in the “woody” tissues of  
673 plants: implications for plant water source, water uptake, and other studies which use the  
674 stable isotopic composition of cellulose. *Geochimica et Cosmochimica Acta* **57**: 3487–3492.
- 675 **Dawson TE, Mambelli S, Plamboeck AH, Templer PH, Tu KP. 2002.** Stable isotopes in  
676 plant ecology. *Annual review of ecology and systematics* **33**: 507–559.
- 677 **De Deurwaerder H, Hervé-Fernández P, Stahl C, Burban B, Petronelli P, Hoffman B,**  
678 **Bonal D, Boeckx P, Verbeeck H. 2018.** Liana and tree below-ground water competition—  
679 evidence for water resource partitioning during the dry season. *Tree Physiology*.
- 680 **Doussan C, Pierret A, Garrigues E, Pagès L. 2006.** Water uptake by plant roots: II—  
681 modelling of water transfer in the soil root-system with explicit account of flow within the  
682 root system—comparison with experiments. *Plant and soil* **283**: 99–117.
- 683 **Ehleringer JR, Dawson TE. 1992.** Water uptake by plants: perspectives from stable isotope  
684 composition. *Plant, Cell & Environment* **15**: 1073–1082.
- 685 **Ellsworth PZ, Williams DG. 2007.** Hydrogen isotope fractionation during water uptake by  
686 woody xerophytes. *Plant and Soil* **291**: 93–107.
- 687 **Epila J, Maes WH, Verbeeck H, Camp J Van, Okullo JBL, Steppe K. 2017.** Plant



688 measurements on African tropical *Maesopsis eminii* seedlings contradict pioneering water use  
689 behaviour. *Environmental and Experimental Botany* **135**: 27–37.

690 **Evaristo J, McDonnell JJ, Scholl MA, Bruijnzeel LA, Chun KP. 2016.** Insights into plant  
691 water uptake from xylem-water isotope measurements in two tropical catchments with  
692 contrasting moisture conditions. *Hydrological Processes* **30**: 3210–3227.

693 **Gartner BL, Bullock SH, Mooney HA, Brown VB, Whitbeck JL. 1990.** Water Transport  
694 Properties of Vine and Tree Stems in a Tropical Deciduous Forest. *American Journal of*  
695 *Botany* **77**: 742–749.

696 **Gerwing JJ, Schnitzer SA, Burnham RJ, Bongers F, Chave J, DeWalt SJ, Ewango CEN,**  
697 **Foster R, Kenfack D, Martínez-Ramos M. 2006.** A standard protocol for liana censuses.  
698 *Biotropica* **38**: 256–261.

699 **Gessler A, Brandes E, Keitel C, Boda S, Kayler ZE, Granier A, Barbour M, Farquhar**  
700 **GD, Treydte K. 2013.** The oxygen isotope enrichment of leaf-exported assimilates—does it  
701 always reflect lamina leaf water enrichment? *New Phytologist* **200**: 144–157.

702 **Goldstein G, Andrade JL, Meinzer FC, Holbrook NM, Cavelier J, Jackson P, Celis A.**  
703 **1998.** Stem water storage and diurnal patterns of water use in tropical forest canopy trees.  
704 *Plant, Cell & Environment* **21**: 397–406.

705 **Gröning M. 2011.** Improved water  $\delta^2\text{H}$  and  $\delta^{18}\text{O}$  calibration and calculation of measurement  
706 uncertainty using a simple software tool. *Rapid Communications in Mass Spectrometry* **25**:  
707 2711–2720.

708 **Hervé-Fernández P, Oyarzún C, Brumbt C, Huygens D, Bodé S, Verhoest NEC, Boeckx**  
709 **P. 2016.** Assessing the ‘two water worlds’ hypothesis and water sources for native and exotic  
710 evergreen species in south-central Chile. *Hydrological Processes* **30**: 4227–4241.



- 711 **Huang C, Domec J, Ward EJ, Duman T, Manoli G, Parolari AJ, Katul GG. 2017.** The  
712 effect of plant water storage on water fluxes within the coupled soil–plant system. *New*  
713 *Phytologist* **213**: 1093–1106.
- 714 **Jackson PC, Cavelier J, Goldstein G, Meinzer FC, Holbrook NM. 1995.** Partitioning of  
715 water-resources among plants of a lowland tropical forest. *Oecologia* **101**: 197–203.
- 716 **De Jong van Lier Q, Van Dam JC, Metselaar K, De Jong R, Duijnsveld WHM. 2008.**  
717 Macroscopic root water uptake distribution using a matric flux potential approach. *Vadose*  
718 *Zone Journal* **7**: 1065–1078.
- 719 **Knipfer T, Cuneo I, Brodersen C, McElrone AJ. 2016.** In-situ visualization of the  
720 dynamics in xylem embolism formation and removal in the absence of root pressure: a study  
721 on excised grapevine stems. *Plant Physiology*: pp-00136.
- 722 **Leuschner C, Coners H, Icke R. 2004.** In situ measurement of water absorption by fine roots  
723 of three temperate trees: species differences and differential activity of superficial and deep  
724 roots. *Tree Physiology* **24**: 1359–1367.
- 725 **Lin G, Sternberg L. 1993.** Hydrogen isotopic fractionation by plant roots during water  
726 uptake in coastal wetland plants. *Stable isotopes and plant carbon-water relations*. Elsevier,  
727 497–510.
- 728 **Mamonov AB, Coalson RD, Zeidel ML, Mathai JC. 2007.** Water and deuterium oxide  
729 permeability through aquaporin 1: MD predictions and experimental verification. *The Journal*  
730 *of general physiology* **130**: 111–116.
- 731 **Martin-Gomez P, Barbeta A, Voltas J, Penuelas J, Dennis K, Palacio S, Dawson TE,**  
732 **Pedro Ferrio J. 2015.** Isotope-ratio infrared spectroscopy: a reliable tool for the investigation  
733 of plant-water sources? *New Phytologist* **207**: 914–927.



- 734 **McKay J. 1988.** Sensitivity and uncertainty analysis using a statistical sample of input values.  
735 *Uncertainty analysis.*
- 736 **McKay MD, Beckman RJ, Conover WJ. 1979.** Comparison of three methods for selecting  
737 values of input variables in the analysis of output from a computer code. *Technometrics* **21**:  
738 239–245.
- 739 **Meißner M, Köhler M, Schwendenmann L, Hölscher D. 2012.** Partitioning of soil water  
740 among canopy trees during a soil desiccation period in a temperate mixed forest.  
741 *Biogeosciences* **9**: 3465–3474.
- 742 **Meunier F, Rothfuss Y, Bariac T, Biron P, Richard P, Durand J-L, Couvreur V,**  
743 **Vanderborght J, Javaux M. 2017.** Measuring and modeling hydraulic lift of *Lolium*  
744 multiflorum using stable water isotopes. *Vadose Zone Journal.*
- 745 **Morris H, Plavcová L, Cvecko P, Fichtler E, Gillingham MAF, Martínez-Cabrera HI,**  
746 **McGlinn DJ, Wheeler E, Zheng J, Ziemińska K. 2016.** A global analysis of parenchyma  
747 tissue fractions in secondary xylem of seed plants. *New Phytologist* **209**: 1553–1565.
- 748 **Orlowski N, Frede HG, Brüggemann N, Breuer L. 2013.** Validation and application of a  
749 cryogenic vacuum extraction system for soil and plant water extraction for isotope analysis. *J.*  
750 *Sens. Sens. Syst* **2**: 179–193.
- 751 **Penna D, Hopp L, Scandellari F, Allen ST, Benettin P, Beyer M, Geris J, Klaus J,**  
752 **Marshall JD, Schwendenmann L. 2018.** Ideas and perspectives: Tracing terrestrial  
753 ecosystem water fluxes using hydrogen and oxygen stable isotopes—challenges and  
754 opportunities from an interdisciplinary perspective. *Biogeosciences.*
- 755 **Phillips DL, Gregg JW. 2003.** Source partitioning using stable isotopes: coping with too  
756 many sources. *Oecologia* **136**: 261–269.



- 757 **R Core Team. 2017.** R: A language and environment for statistical computing. R Foundation  
758 for Statistical Computing.
- 759 **Rothfuss Y, Javaux M. 2017.** Reviews and syntheses: Isotopic approaches to quantify root  
760 water uptake: a review and comparison of methods. *Biogeosciences* **14**: 2199.
- 761 **Rüdinger M, Hallgren SW, Steudle E, Schulze E-D. 1994.** Hydraulic and osmotic  
762 properties of spruce roots. *Journal of Experimental Botany* **45**: 1413–1425.
- 763 **Salleo S, Trifilò P, Esposito S, Nardini A, Gullo MA Lo. 2009.** Starch-to-sugar conversion  
764 in wood parenchyma of field-growing *Laurus nobilis* plants: a component of the signal  
765 pathway for embolism repair? *Functional Plant Biology* **36**: 815–825.
- 766 **Sands R, Fiscus EL, Reid CPP. 1982.** Hydraulic properties of pine and bean roots with  
767 varying degrees of suberization, vascular differentiation and mycorrhizal infection.  
768 *Functional Plant Biology* **9**: 559–569.
- 769 **Secchi F, Pagliarani C, Zwieniecki MA. 2017.** The functional role of xylem parenchyma  
770 cells and aquaporins during recovery from severe water stress. *Plant, cell & environment* **40**:  
771 858–871.
- 772 **Steppe K, Lemeur R. 2004.** An experimental system for analysis of the dynamic sap-flow  
773 characteristics in young trees: results of a beech tree. *Functional Plant Biology* **31**: 83–92.
- 774 **Steppe K, De Pauw DJW, Doody TM, Teskey RO. 2010.** A comparison of sap flux density  
775 using thermal dissipation, heat pulse velocity and heat field deformation methods.  
776 *Agricultural and Forest Meteorology* **150**: 1046–1056.
- 777 **Steudle E, Meshcheryakov AB. 1996.** Hydraulic and osmotic properties of oak roots.  
778 *Journal of Experimental Botany* **47**: 387–401.
- 779 **Vargas AI, Schaffer B, Yuhong L, Sternberg L da SL. 2017.** Testing plant use of mobile



- 780 vs immobile soil water sources using stable isotope experiments. *New Phytologist* **215**: 582–  
781 594.
- 782 **Vogel T, Dohnal M, Dusek J, Votrubova J, Tesar M. 2013.** Macroscopic modeling of plant  
783 water uptake in a forest stand involving root-mediated soil water redistribution. *Vadose Zone*  
784 *Journal* **12**.
- 785 **Volkman THM, Kühnhammer K, Herbstritt B, Gessler A, Weiler M. 2016.** A method  
786 for in situ monitoring of the isotope composition of tree xylem water using laser spectroscopy.  
787 *Plant, cell & environment* **39**: 2055–2063.
- 788 **Walker CD, Richardson SB. 1991.** The use of stable isotopes of water in characterizing the  
789 source of water in vegetation. *Chemical Geology* **94**: 145–158.
- 790 **Wershaw RL, Friedman I, Heller SJ, Frank PA. 1966.** Hydrogen isotopic fractionation of  
791 water passing through trees. *Advances in organic geochemistry*: 55.
- 792 **White JWC, Cook ER, Lawrence JR, Broecker WS. 1985.** The D/H ratios of sap in trees -  
793 implications for water sources and tree-ring D/H ratios. *Geochimica et Cosmochimica Acta*  
794 **49**: 237–246.
- 795 **De Wispelaere L, Bodé S, Hervé-Fernández P, Hemp A, Verschuren D, Boeckx P. 2016.**  
796 Plant water resource partitioning and xylem-leaf deuterium enrichment in a seasonally dry  
797 tropical climate. *Biogeosciences Discuss.* **2016**: 1–26.
- 798 **Yakir D. 1992.** Variations in the natural abundance of oxygen-18 and deuterium in plant  
799 carbohydrates. *Plant, Cell & Environment* **15**: 1005–1020.
- 800 **Yang Q, Xiao H, Zhao L, Zhou M, Li C, Cao S. 2010.** Stable isotope techniques in plant  
801 water sources: a review. *Sciences in Cold and Arid Regions* **2**: 112–122.
- 802 **Zhao L, Wang L, Cernusak LA, Liu X, Xiao H, Zhou M, Zhang S. 2016.** Significant



803 difference in hydrogen isotope composition between xylem and tissue water in *Populus*  
804 *euphratica*. *Plant, Cell & Environment* **39**: 1848–1857.

805 **Zhao L, Wang L, Liu X, Xiao H, Ruan Y, Zhou M. 2014.** The patterns and implications of  
806 diurnal variations in the  $\delta$ -excess of plant water, shallow soil water and air moisture.

807 **Zhao L, Xiao H, Zhou J, Wang L, Cheng G, Zhou M, Yin L, McCabe MF. 2011.** Detailed  
808 assessment of isotope ratio infrared spectroscopy and isotope ratio mass spectrometry for the  
809 stable isotope analysis of plant and soil waters. *Rapid Communications in Mass Spectrometry*  
810 **25**: 3071–3082.

811 **Zimmermann U, Ehhalt D, Münnich K. 1967.** Soil-Water movement and  
812 evapotranspiration: changes in the isotopic composition of the water. Conference on Isotopes  
813 in Hydrology. Vienna, 567-585.

814

815



816 **Tables**

817 **Table 1.** Nomenclature.

Symbol	Description	Unit
$A_{R,i}$	The absorptive root area distribution over soil layer $i$	$\text{m}^2$
$A_{Rtot}$	The plants' total active fine root surface area	$\text{m}^2$
$A_{SAPWOOD}$	Sapwood area	$\text{m}^2$
$A_x$	Total lumen area	$\text{m}^2$
$b$	Shape parameter for the soil hydraulic properties (Clapp & Hornberger, 1978)	dimensionless
$B_i$	The overall root length density distribution per unit of soil, not necessarily limited to the focal plant.	$\text{m m}^{-3}$
$\delta^2H_{X,0,t}$	Isotope composition of plant xylem water at stem base at time $t$	in ‰ VSMOW
$\delta^2H_{X,h,t}$	Isotope composition of plant xylem water at height $h$ and time $t$	in ‰ VSMOW
$\delta^2H_{S,i}$	Isotope composition of soil water of the $i^{\text{th}}$ soil layer (constant over time)	in ‰ VSMOW
$\delta_{\text{sample}}$	Isotope composition of water within a sample	in ‰ VSMOW
$\Delta\hat{\Psi}_{i,t}$	Estimated water potential gradient between stem base and the $i^{\text{th}}$ soil layer at time $t$ derived from Eq. (8)	$\text{m}$
$\Delta\Psi_{i,t}$	Soil water potential gradient between soil and roots at the $i^{\text{th}}$ soil layer at time $t$	$\text{m H}_2\text{O}$
$\epsilon^2\text{H}_X ; \epsilon^{18}\text{O}_X$	Normalized isotope composition of plant xylem water	in ‰ VSMOW
$f_{i,t}$	Fraction of water taken up in the $i^{\text{th}}$ soil layer at time $t$	dimensionless
$h$	Measurement height	$\text{m}$
$i$	Soil layer index	dimensionless
$i\text{-H}_2\text{O-}xyl$	Isotope composition of plant xylem water	in ‰ VSMOW
$k_i$	Soil-root conductance of the $i^{\text{th}}$ soil layer	$\text{s}^{-1}$
$K_{max}$	Maximum soil hydraulic conductivity	$\text{m s}^{-1}$
$k_R$	Effective root radial conductivity	$\text{s}^{-1}$
$k_S$	The conductance associated with the radial water flow between the soil and the root surface	$\text{s}^{-1}$
$K_{S,i}$	Soil hydraulic conductivity at the $i^{\text{th}}$ soil layer	$\text{m s}^{-1}$
$\ell$	The approximated radial pathway length of water flow between bulk soil and root surface	$\text{m}$
LF	Lumen fraction per unit sapwood area	$\text{m}^2 \text{m}^{-2}$
$n$	Number of unique contributing water sources	#
$\Psi_{sat}$	Soil water potential at soil saturation	$\text{m}$
$\Psi_{S,i,t}$	Soil water potential of the $i^{\text{th}}$ soil layer at time $t$	$\text{m}$
$\Psi_{X,0,t}$	Water potential at the base of the plant stem at time $t$	$\text{m}$



$R$	Heavy to light isotope ratio measured in the sample or standard	%
$RWU_{i,t}$	Net amount of water entering and leaving the root tissues per unit of time in the $i^{\text{th}}$ soil layer at time $t$	$\text{m}^3 \text{s}^{-1}$
$SF_t$	Instantaneous sap flow at time $t$	$\text{m}^3 \text{s}^{-1}$
$SF_S$	Sap flow velocity, calculated as the sap flow per sapwood area	$\text{m h}^{-1}$
$SF_V$	True sap flux density, calculated as the sap flow per lumen area	$\text{m h}^{-1}$
$\tau$	Delay before the isotope composition of xylem water at stem base reaches stem height $h$	s
$\theta_{sat}$	Soil moisture content at soil saturation	$\text{m}^3 \text{m}^{-3}$
$\theta_{S,i,t}$	Soil moisture content of the $i^{\text{th}}$ soil layer at time $t$	$\text{m}^3 \text{m}^{-3}$
$z_i$	Soil depth of the $i^{\text{th}}$ soil layer	m

818

819



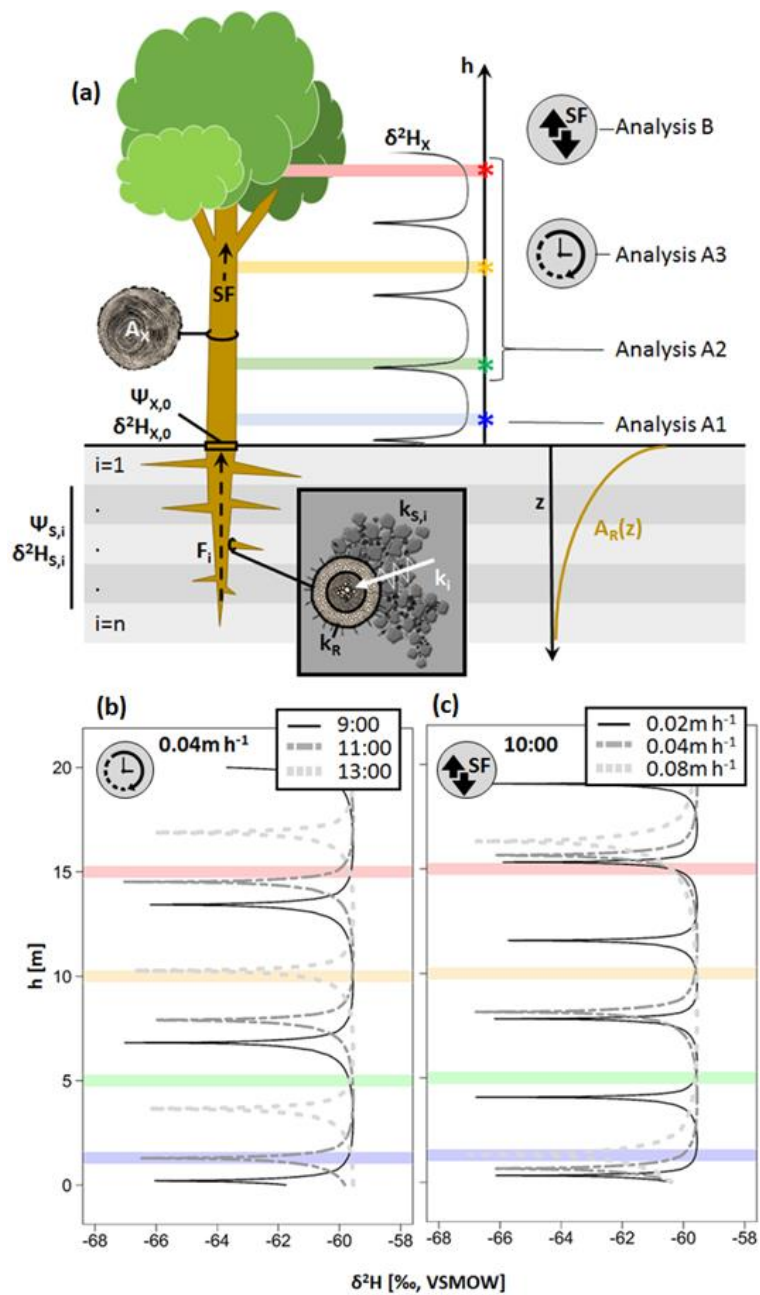
820  
 821

**Table 2.** Sampled liana and tree individuals, provided with their species, respective diameter at breast height (DBH, in cm) and their  $\delta^2H$  and  $\delta^{18}O$  ranges (in ‰, VSMOW) measured per individual.

Code	Growth form	DBH [cm]	Family	Species name	$\delta^2H_X$ -range [in ‰, VSMOW]	$\delta^{18}O_X$ -range [in ‰, VSMOW]
SP1	Tree	15.6	Moraceae	<i>Coussapoa</i> sp.	-30.1; -25.5	-2.8; -2.6
SP2	Tree	50.9	Fabaceae	<i>Youacapoua americana</i>	-23.9; -18.1	-3.1; -2.2
SP3	Tree	44.6	Vochysiaceae	<i>Erisma nitidum</i>	-27.7; -20.8	-3.2; -1.9
SP4	Tree	26.1	Sapotaceae	<i>Micropholis guyanensis</i>	-29.8; -28.0	-3.0; -2.9
SP5	Tree	21.0	Anacardiaceae	<i>Tapirira guyanensis</i>	-31.1; -18.0	-3.2; -2.2
SP6	Tree	49.7	Fabaceae	<i>Albizia pedicellaris</i>	-26.9; -22.1	-3.2; -2.6
SP1	Liana	2.8	Polygonaceae	<i>Coccoloba</i> sp.	-27.9; -20.7	-3.9; -2.3
SP2	Liana	2.7	Convolvulaceae	sp.	-29.3; -24.0	-4.4; -2.9
SP3	Liana	0.8	Moraceae	sp.	-40.8; -22.6	-4.5; -2.3
SP4	Liana	3.8	Combretaceae	cf. <i>rotundifolium</i> Rich.	-23.6; -15.2	-2.9; -2.0
SP5	Liana	0.7	Convolvulaceae	<i>Maripa</i> cf. <i>violacea</i>	-31.6; -19.7	-3.8; -2.7
SP6	Liana	3.8	Convolvulaceae	<i>Maripa</i> sp.	-35.3; -24.4	-4.8; -3.1



824 **Figures**

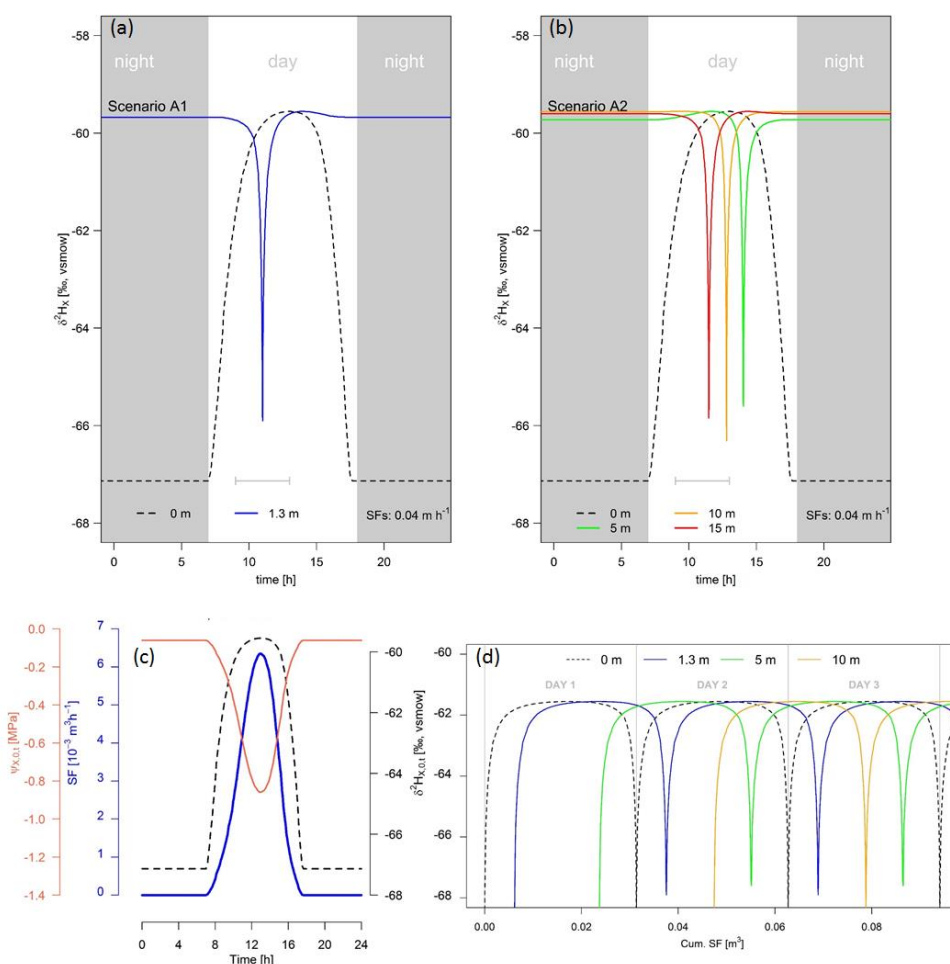


825

826



827 **Fig. 1. Panel a:** Schematic representation of the model and considered analysis detailed in the  
828 text. **Panel b:** Model outputs for model analysis A3 representing the deuterium isotope  
829 composition of xylem water ( $\delta^2\text{H}_X$ ) as a function of the tree height simulated for different  
830 sampling times (9:00, 11:00 and 13:00). The modeled tree has an average daily sap flux density  
831 of  $0.04 \text{ m h}^{-1}$  ( $\text{SF}_S$ ), which corresponds to an average daily true sap flux density of  $0.28 \text{ m h}^{-1}$   
832 ( $\text{SF}_V$ ). Panel c: Model outputs for model analysis B where  $\delta^2\text{H}_X$  in relation with stem height is  
833 shown at 10:00 h, but parameterized with distinct average sap flux density, i.e. 0.08, 0.04 and  
834  $0.02 \text{ m h}^{-1}$  (corresponding to an average true sap flux density  $\text{SF}_V$  of 0.56, 0.28 and  $0.14 \text{ m h}^{-1}$ ,  
835 respectively). The standard parameterization used for both study analysis is detailed in Table  
836 S1.



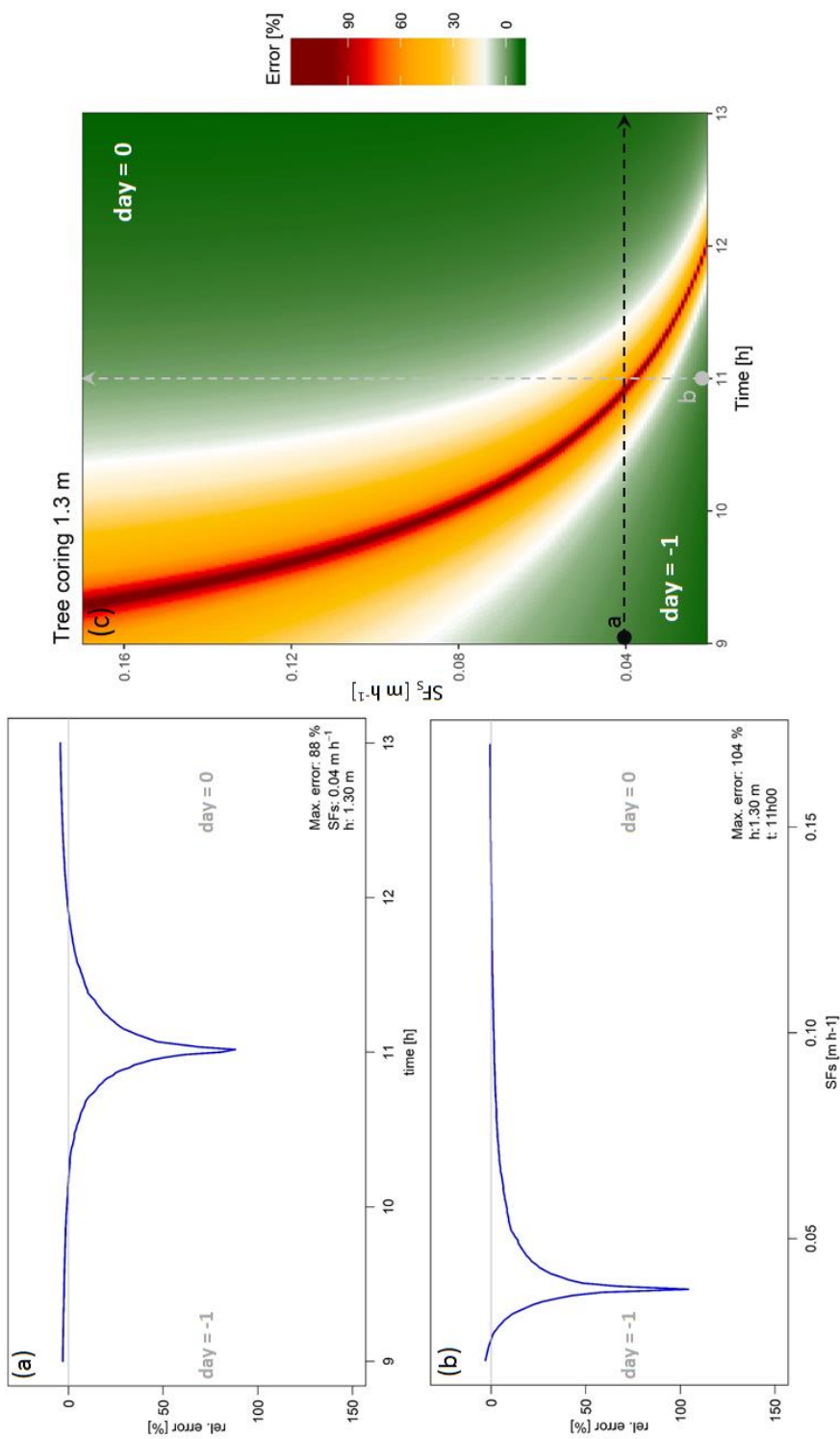
837

838 **Fig. 2. Panel a & b:** Diurnal patterns of simulated in deuterium isotope composition of plant  
839 xylem water ( $\delta^2H_X$ ) fluctuation as a function of time for various tree heights. The modeled tree  
840 has an average daily sap flux density ( $SF_S$ ) of  $0.04 \text{ m h}^{-1}$ , which corresponds to an average daily  
841 true sap flux density of  $0.28 \text{ m h}^{-1}$  ( $SF_V$ ), and the standard parameterization is detailed in Table  
842 S1. Panel (a) shows analysis A1 output where diurnal  $\delta^2H_X$  patterns are provided at stem base  
843 (0 m, black dashed line) and at general tree coring height at breast level, i.e. at 1.3 m (blue).  
844 Panel (b) shows analysis A2 outputs demonstrating diurnal patterns in  $\delta^2H_X$  within a standard  
845 tree at various heights, i.e. at 0 m (black dotted), 5 m (green), 10 m (orange) and 15 m (red).



846 These heights represent random branch sample collection and conform to the standard practice  
847 of RWU assessment. Grey lines with whiskers indicate the common sampling period (9:00 until  
848 13:00) according to standard practice. **Panel c:** Sap flow rate ( $SF$ , blue line), deuterium isotope  
849 composition of xylem water ( $\delta^2H_{X,0,t}$  black dashed line) and water potential at stem base  
850 ( $\Psi_{X,0,t}$ , red line) are shown over the period of a single day. **Panel d:** Simulated  $\delta^2H_X$  fluctuations  
851 in function of the cumulative sap flow volume measured at various heights: stem base (0 m,  
852 black dashed), 1.3 m (blue), 5 m (green) and 10 m (red). Days are delineated by grey vertical  
853 lines.

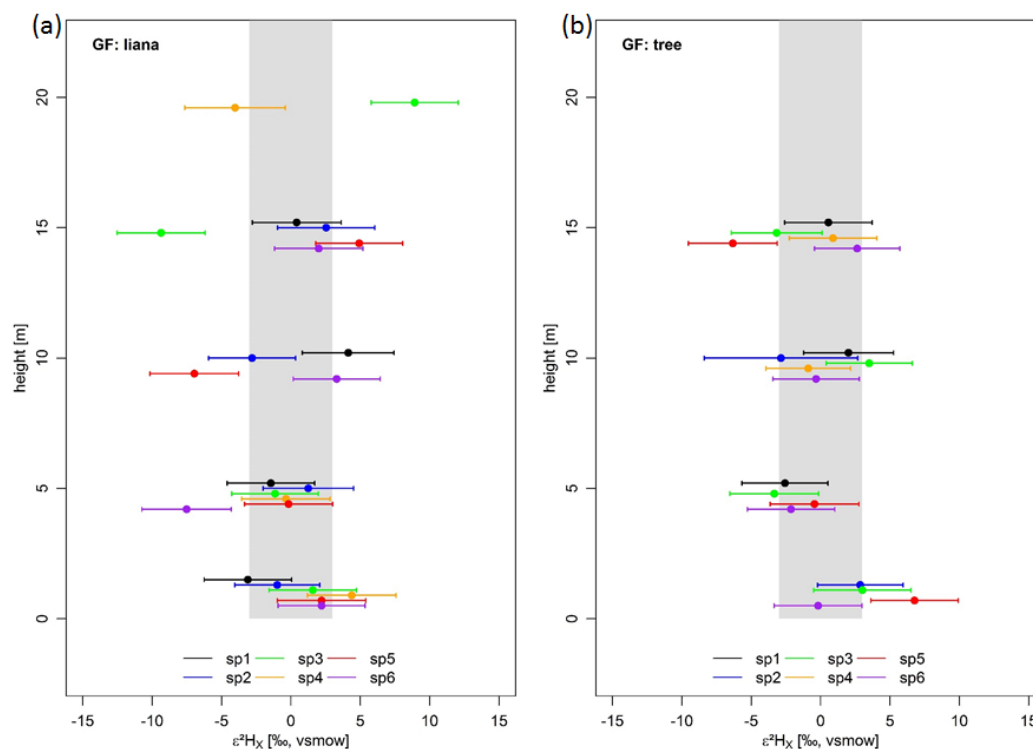
854





856 **Fig. 3.** a) Relative error on the inferred root water uptake (RWU) depth (i.e. bias between the  
857 average daily and the instantaneous derived RWU depth), for a tree measured at standard tree  
858 coring height (i.e. 1.30 m) which has a sap flux density ( $SF_S$ ) of  $0.04 \text{ m h}^{-1}$  (i.e.  $SF_V = 0.28 \text{ m}$   
859  $\text{h}^{-1}$ ), over the common sampling period (9:00 until 13:00). b) Relative error on the inferred  
860 RWU depth considering a tree measured at standard tree coring height (1.30 m) at 11:30, but  
861 which differs in  $SF_S$ . c) Relative error on the inferred RWU depth over the duration of the  
862 common sampling period (9:00 until 13:00) and over a range of potential  $SF_S$  (in  $\text{m h}^{-1}$ ) –  
863 corresponding to  $SF_V$  range of  $0.15\text{--}1.25 \text{ m h}^{-1}$ . Dotted lines a (black) and b (grey) correspond  
864 to their respective representation in panel a and b. day= -1 and day= 0 indicate whether the  
865 derived RWU depth error corresponds to the previous or current day of measurement.

866



867

868 **Fig. 4.** Field measurements of normalized intra-individual  $\delta^2H_x$  ( $\epsilon^2H_x$ ) for six lianas (panel a)  
869 and six trees (panel b). Individuals are provided in different colors; species names can be  
870 derived from Table 2. Error whiskers are the combination of potential extraction ( $\pm 3\text{‰}$ ) and  
871 measurement errors of the isotope analyzer. The full grey envelope delineates the acceptable  
872 variance from the stem mean (i.e.  $3\text{‰}$ ) according to the standard assumption of no variance  
873 along the length of a lignified plant, i.e the null model.

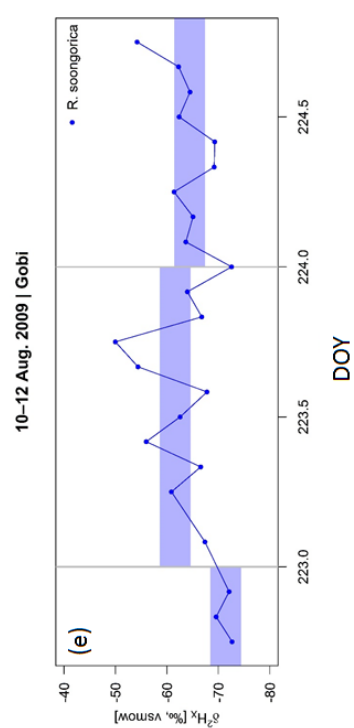
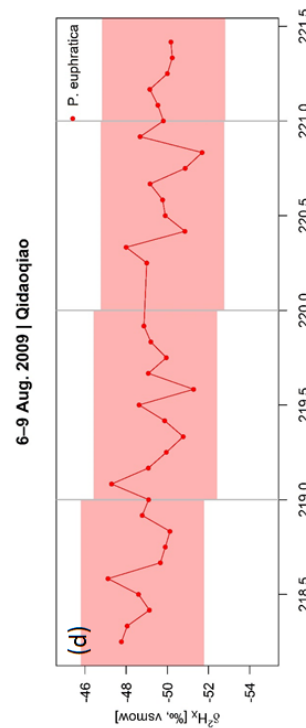
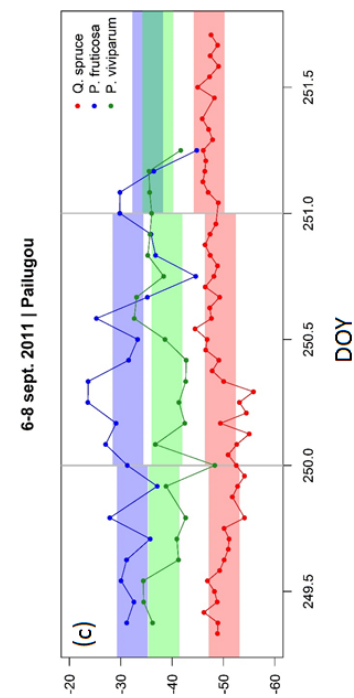
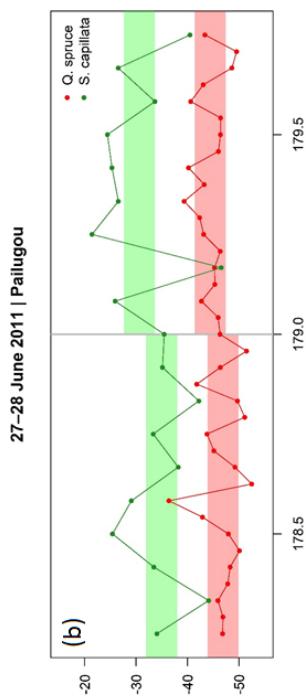
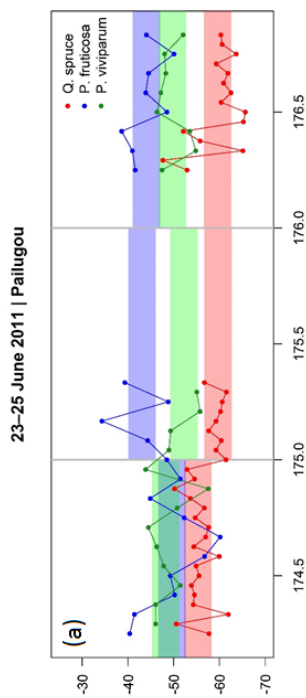
874

875

876



Species	Max. diurnal $\delta^2\text{H}_x$ range [% <sub>v</sub> in vsmow]	Growth form	Color code
<i>Q. Spruce</i>	18.0	Tree	Red
<i>P. euphratica</i>	4.0	Tree	Blue
<i>P. fruticosa</i>	21.0	Shrub	Green
<i>R. soongorica</i>	18.4	Shrub	Blue
<i>P. viviparum</i>	15.7	Herb	Red
<i>S. capillata</i>	25.2	Herb	Green



$\delta^2\text{H}_x$  [% in vsmow]



878 **Fig. 5.** High temporal field measurements of deuterium isotope composition of xylem water  
879 ( $\delta^2H_X$ ) of two tree (red, stem samples), two shrub (blue, stem samples) and two herb (green,  
880 root samples) species sampled in the Heihe River Basin (northwestern China) shown for the  
881 respective measurement periods. Timing and location of sampling are provided in the panel  
882 titles. The full colored envelope per respective species delineates the acceptable variance from  
883 the stem mean (i.e. 3‰) according to the standard assumption of no variance along the length  
884 of a lignified plant. Grey vertical lines mark the transition of days. The table provides the  
885 maximum measured diurnal  $\delta^2H_X$  range per species.

886